

Numerical analytic continuation: answers to well-posed questions

Olga Goulko

Department of Physics, University of Massachusetts, Amherst, MA 01003, USA

Andrey S. Mishchenko

*RIKEN Center for Emergent Matter Science (CEMS),
2-1 Hirosawa, Wako, Saitama, 351-0198, Japan and*

National Research Center “Kurchatov Institute,” 123182 Moscow, Russia

Lode Pollet

*Department of Physics, Arnold Sommerfeld Center for Theoretical Physics,
University of Munich, Theresienstrasse 37, 80333 Munich, Germany*

Nikolay Prokof'ev

Department of Physics, University of Massachusetts, Amherst, MA 01003, USA

Department of Physics, Arnold Sommerfeld Center for Theoretical Physics,

University of Munich, Theresienstrasse 37, 80333 Munich, Germany and

National Research Center “Kurchatov Institute,” 123182 Moscow, Russia

Boris Svistunov

Department of Physics, University of Massachusetts, Amherst, MA 01003, USA

National Research Center “Kurchatov Institute,” 123182 Moscow, Russia and

Wilczek Quantum Center, Zhejiang University of Technology, Hangzhou 310014, China

(Dated: April 5, 2024)

We formulate the problem of numerical analytic continuation in a way that lets us draw meaningful conclusions about properties of the spectral function based solely on the input data. Apart from ensuring consistency with the input data (within their error bars) and the *a priori* and *a posteriori* (conditional) constraints, it is crucial to reliably characterize the accuracy—or even ambiguity—of the output. We explain how these challenges can be met with two approaches: stochastic optimization with consistent constraints and the modified maximum entropy method. We perform illustrative tests for spectra with a double-peak structure, where we critically examine which spectral properties are accessible and which ones are lost. For an important practical example, we apply our protocol to the Fermi polaron problem.

PACS numbers: 02.70.-c, 71.15.Dx, 71.28.+d, 71.10.Fd

I. INTRODUCTION

Numerous problems in science, from spectral analysis to image processing, require that we restore properties of a function $A(z)$ from a set of integrals

$$g_n = G[n, A] \equiv \int_{-\infty}^{\infty} dz K(n, z) A(z), \quad n = 1, \dots, N, \quad (1)$$

where $K(n, z)$ is a known kernel and $\{g_n\}$ is a finite set of experimental or numerical input data with error bars. An important class of such problems—known as numerical analytic continuation (NAC)—deals with “pathological” kernels featuring numerous eigenfunctions with anomalously small eigenvalues. An archetypal NAC problem is the numerical spectral analysis at zero temperature, where the challenge is to restore the non-negative spectral function $A(z \geq 0)$ satisfying the equation

$$g_n = \int_0^{\infty} dz e^{-z\tau_n} A(z), \quad (2)$$

from numerical data for $g_n = g(\tau_n \geq 0)$.

The NAC problem is often characterized as *ill-posed*. Mathematically, the near-degeneracy of the kernel implies two closely related circumstances: (i) the absence of the resolvent, and (ii) a continuum of solutions satisfying the input data within their error bars (even when integrals over z are replaced with finite sums containing less or equal to N terms). Nowadays, the first circumstance is merely a minor technical problem, as there exists a number of methods allowing one to find solutions to (1) without compromising the error bars of g_n .

The second circumstance—the ambiguity of the solution—is a more essential problem. It is clear that if one formulates the goal as to restore $A(z)$ as a continuous curve, or to determine its value on a given grid of points, then the goal cannot be reached as stated, irrespective of the properties of the kernel $K(n, z)$. The input data set is finite and noisy, thereby introducing a natural limit on the resolution of fine structures in $A(z)$.

Fortunately, the above-formulated goal has little to do with the practical world. In an experiment, all devices are characterized by a finite resolution function and the data they collect always correspond to *integrals*. The

data are processed by making certain *assumptions* about the underlying function. This motivates an alternative formulation of the NAC goal involving integrals of $A(z)$ that render the problem well-defined. With additional assumptions about the smoothness and other properties of $A(z)$ behind these integrals, consistent with both *a priori* and *a posteriori* knowledge, the ambiguity of the solution can be substantially suppressed. The simplest setup is as follows:

Given a set of finite intervals $\{\Delta_m\}$, determine the integrals of the spectral function over these intervals:

$$i_m = \Delta_m^{-1} \int_{z \in \Delta_m} dz A(z), \quad m = 1, \dots, M, \quad (3)$$

along with the corresponding dispersions of fluctuations $\{\sigma_m\}$ (straightforwardly extendable to the dispersion correlation matrix $\{\sigma_{mm'}\}$).

Naively one might think that nothing is achieved by going from the integrals in (1) to the integrals in (3) because the latter have exactly the same form with the kernel $\bar{K}(m, z) = \Delta_m^{-1}$ for $z \in \Delta_m$ and zero otherwise (other forms of the “resolution function” $\bar{K}(m, z)$ are discussed in Sec. II):

$$i_m = I[m, A] = \int_{-\infty}^{\infty} dz \bar{K}(m, z) A(z), \quad m = 1, \dots, M. \quad (4)$$

This impression, however, is false because kernel properties are at the heart of the problem. If for appropriately small intervals (sufficiently small to resolve the variations of $A(z)$), the uncertainties for i_m remain small, then one can draw reliable conclusions for the underlying behavior of $A(z)$ itself. The difference between “good” (e.g. as in Fourier transforms) and pathological kernels is that for the latter, due to the notorious saw-tooth instability, the uncertainties for i_m quickly become too large for a meaningful analysis of fine structures in $A(z)$.

To obtain a solution from the integrals (3), one has to invoke the notion of *conditional knowledge*. The most straightforward approach is to set the spectral function values at the middle points z_m of the intervals Δ_m to $A_{\text{fin}}(z_m) = i_m$. This is only possible if the intervals can be made appropriately narrow without losing accuracy for the integrals. With this approach we assume that the function is nearly linear over the intervals in question. This is a typical procedure for experimental data. Quantifying the error bar on $A_{\text{fin}}(z_m)$ necessarily involves *two* numbers: the “vertical” dispersion σ_m is directly inherited from i_m , and the “horizontal” error bar $\Delta_m/2$ represents the interval half-width.

The reader should be aware of two issues regarding such error bars. First, the error bars for different points are not independent but contain significant multi-point correlations. For example, an unrestricted integral

$\int dz A(z)$ is typically known with an accuracy that is orders of magnitude better than what would be predicted by the central limit theorem if this integral is represented by a finite sum of integrals over nonoverlapping intervals. Second, the errors are not necessarily distributed as a Gaussian. Atypical fluctuations can have a significant probability and their analysis should not be avoided as the actual physical solution may well be one of them. To this end, it is important to explore the minimal and maximal values that the integral i_m can take, and check that these are not significantly different from the typical value of i_m . In certain cases this criterion cannot be met without increasing the intervals Δ_m to an extent when the assumption of linearity of $A(z)$ becomes uncontrolled, implying that an important piece of information about the shape of $A(z)$ in this interval is missing. A characteristic example that plays a key role in the subsequent discussion is presented in Fig. 1, where the challenge is to extract the shape of the second peak.

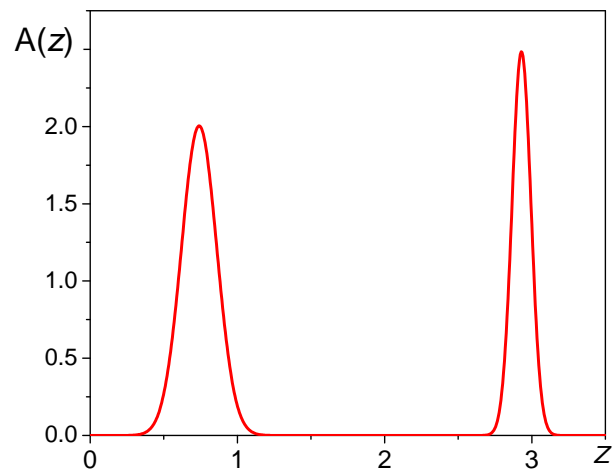


FIG. 1. Challenging example of a spectrum $A(z)$ for the NAC problem (2). As shown in the main part of the text, the significant width of the first peak makes it essentially impossible to controllably restore the width of the second peak, even with small relative error bars ($\sim 10^{-5}$) on g_n . On the other hand, the first two moments of the second peak, characterizing its weight and position, can be extracted reliably.

In the more sophisticated approach used in this work, the values of $A_{\text{fin}}(z_m)$ can be further optimized (without compromising the accuracy of the solution with respect to g_n) to produce a smooth curve. This protocol has the additional advantage of eliminating minima, maxima, gaps, and sharp features that are not guaranteed to exist by the quality of input data. The nature of the problem is such that very narrow peaks (or gaps) with tiny spectral weight can always be imagined to be present (for narrow intervals they will certainly emerge due to the saw-tooth instability). Our philosophy with respect to these features is to erase them *within the established error bounds* and obtain a solution that is insensitive to the interval parameters.

Having established a smooth solution, one may nevertheless ask whether a particular feature of the solution can, in principle, have significantly different properties. For example, if the NAC procedure suggests a peak, one may wonder if the true spectral function could have a much narrower peak with the same area, and if so, what is its smallest possible width. A NAC protocol should be able to answer this type of question fast and reliably. In this work, we explain how these goals can be achieved in practice. Many technical details of the protocol that we propose to abbreviate as SOCC (Stochastic Optimization with Consistent Constraints) were already published in Refs. 1–3 as separate developments. The crucial advances here are (i) the final formulation based on integrals of the spectral function, and (ii) the idea of working with linear combinations of pre-calculated “basic” solutions. The latter allows one to readily apply consistent constraints without compromising the error bars on the input data. Consistent constraints are also crucial for assessing what features can be resolved and what information is unrecoverable.

In what follows, the term “consistent constraints” applies to (i) the general principle of utilizing the *a priori* and revealing the *a posteriori* (conditional) knowledge without compromising the error bars of the input data and (ii) a particular set of numerical procedures based on ideas respecting this principle. Our SOCC protocol involves two different consistent-constraint procedures. The first one, borrowed from the NAC method of Ref. 3, is now used solely to (dramatically!) enhance the performance of the stochastic-optimization part of the protocol searching for basic solutions. The most important consistent-constraint procedure is used to post-process the set of basic solutions.

The paper is organized as follows. In Sec. II we describe the SOCC method consisting of three distinct stages, and explain how a smooth solution can be obtained without any bias with respect to solving Eq. (1) and analyzed for possible atypical deformations. In Sec. III we briefly review the maximum entropy method (MEM).^{4–9} In Sec. IV we explore what SOCC and MEM methods predict for the test spectral function shown in Fig. 1, and how one should analyze the final solution with respect to its possible smooth transformations. In Sec. V we apply our findings to the physical spectral function of the resonant Fermi polaron.^{10–17} We conclude in Sec. VI.

II. STOCHASTIC OPTIMIZATION WITH CONSISTENT CONSTRAINTS

The formulation of the SOCC method is relatively simple and consists of three parts:

1. Finding a large set of solutions $A_j(z)$ [$j = 1, \dots, J \gg 1$] to Eq. (1) that satisfy the input data within their error bounds. In what follows we call them “basic” solutions. Basic solutions are not

biased in any way to be smooth or to satisfy any other requirements based on knowledge about the problem outside of Eq. (1). The irregularity of basic solutions embodies what is referred to as an ill-posed problem. In subsection II A we briefly explain how these solutions are found by the stochastic optimization procedure (most technical details were published previously in Refs. 1 and 2) and how the consistent constraints method³ is used to improve drastically the speed of the stochastic optimization protocol.

2. Using the basic solutions $A_j(z)$ to compute the integrals (4) with a different kernel $\bar{K}(m, z)$. There are several choices here. One of them is given by Eq. (3) and amounts to computing integrals from $A_j(z)$ over finite intervals $\{\Delta_m\}$ centered at $\{z_m\}$. However, one is also free to consider normalized continuous kernels with unrestricted integration over z , such as Lorentzian (or Gaussian) shapes centered at points $\{z_m\}$ with the width $\{\Delta_m\}$ at half-height, e.g.,

$$\bar{K}(m, z) = \frac{\Delta_m/\pi}{(z - z_m)^2 + \Delta_m^2}. \quad (5)$$

Thus obtained sets of integrals $\{i_m^{(j)}\}$ are then used straightforwardly to compute averages

$$i_m = J^{-1} \sum_{j=1}^J i_m^{(j)}, \quad (6)$$

and dispersions¹⁸

$$\sigma_m^2 = J^{-1} \sum_{j=1}^J \left(i_m^{(j)} - i_m \right)^2. \quad (7)$$

To characterize possible two-point correlations, one should compute the correlation matrix

$$\sigma_{mm'} = J^{-1} \sum_{j=1}^J \left(i_m^{(j)} - i_m \right) \left(i_{m'}^{(j)} - i_{m'} \right). \quad (8)$$

Strictly speaking, there is no reason to stop characterizing correlations at the two-point level. One may proceed with computing multi-point averages but the effort quickly becomes expensive and the outcome cannot be presented in a single plot. An alternative “visualization” of multi-point correlations is discussed in subsection II B.

3. Interpreting the result. The simplest interpretation and an estimate of the dispersion for typical fluctuations is to assume that $A(z)$ is nearly linear over the range of each interval. This leads to the solution $A_{\text{fin}}(z_m) = i_m$ with vertical and horizontal “error bars” $\sigma_m^{(v)} = \sigma_m$ and $\sigma_m^{(h)} = \Delta_m/2$. The vertical error bars may be overestimated because fluctuations at different points are correlated. However, as explained in the Introduction, the

correct answer may correspond to some atypical shape, and this possibility has to be addressed as well.

An alternative protocol, discussed in subsection II B, determines the final solution by selecting a superposition of basic solutions

$$A_{\text{fin}}(z) = \sum_{j=1}^J c_j A_j(z), \quad \sum_{j=1}^J c_j = 1, \quad (9)$$

such that $A(z)$ remains non-negative (with high accuracy) and the coefficients c_j are optimized to impose smooth behavior or any other “conditional knowledge”. Formally, the simplest interpretation corresponds to $c_j = 1/J$.

A. Search for basic solutions

The search for basic solutions relies on the minimization of

$$\chi^2 = N^{-1} \sum_{n=1}^N \left(\frac{g_n - G[n, A]}{\delta_n} \right)^2, \quad (10)$$

where δ_n is the error of the g_n value. Without loss of generality, we assume that the components of the vector $\vec{g} = (g_1, g_2, \dots)$ are uncorrelated; otherwise, one has to perform a rotation to the eigenvector basis of the two-point correlation matrix $\langle (g_n - \langle g_n \rangle)(g'_n - \langle g'_n \rangle) \rangle$ where the components of \vec{g} become statistically independent. This linear transformation leads to an equation that has exactly the same form as (1) with a rotated kernel. We choose a maximal tolerance χ_c of order unity and search for functions $A(z) > 0$ with $\chi^2 < \chi_c^2$, which are then added to the set of basic solutions for further processing.

Information about the input data is limited to the objective function (10). Truly unbiased methods should not assume anything about $A(z)$ that is not part of exact knowledge, such as the predetermined grid of points, and the number and parameters of peaks/gaps. In the stochastic optimization method of Refs. 1 and 2, each solution is represented by a set of positive-definite rectangular shapes (the δ -function can be viewed as the limiting case of an infinitely narrow and infinitely high rectangular shape with fixed area), which are allowed to have multiple overlaps, see panel (a) in Fig 2. More precisely, a solution is represented as a sum

$$A(z) = \sum_{r=1}^R \eta_{\{P_r\}}(z) \quad (11)$$

of rectangles $\{P_r\} = \{h_r, w_r, c_r\}$,

$$\eta_{\{P_r\}}(z) = \begin{cases} h_r, & z \in [c_r - w_r/2, c_r + w_r/2], \\ 0, & \text{otherwise,} \end{cases} \quad (12)$$

where $h_r > 0$, $w_r > 0$, and c_r are the height, width, and center of the rectangle P_r , respectively. In what follows we refer to

$$\mathcal{C} = \{\{P_r\}, r = 1, \dots, R\}, \quad (13)$$

as a “configuration.” All rectangles are restricted to the specified range of the $A(z)$ support, $[z^{(\min)}, z^{(\max)}]$; i.e., for all rectangles $c_r - w_r/2 > z^{(\min)}$ and $c_r + w_r/2 < z^{(\max)}$. The spectrum normalization is given by $\sum_{r=1}^R h_r w_r = N_0$, and $G[n, A]$ in Eq. (1) can be written as

$$G[n, A] = \sum_{r=1}^R \mathcal{K}(n, r) h_r, \quad (14)$$

where

$$\mathcal{K}(n, r) = \int_{c_r - w_r/2}^{c_r + w_r/2} dz K(n, z). \quad (15)$$

The number of rectangles and all continuous parameters characterizing their position, width, and height are found by minimizing the objective (10). Optimization starts from a randomly generated set of rectangles, and finds a large number of dissimilar basic solutions $A_j(z)$ with $\chi^2 < \chi_c^2$. More precisely, the search is based on a chain of randomly chosen updates over the configuration space of shapes which fully explore the saw-tooth fluctuations of basic solutions. This is important for the successful elimination of noise in the final solution.

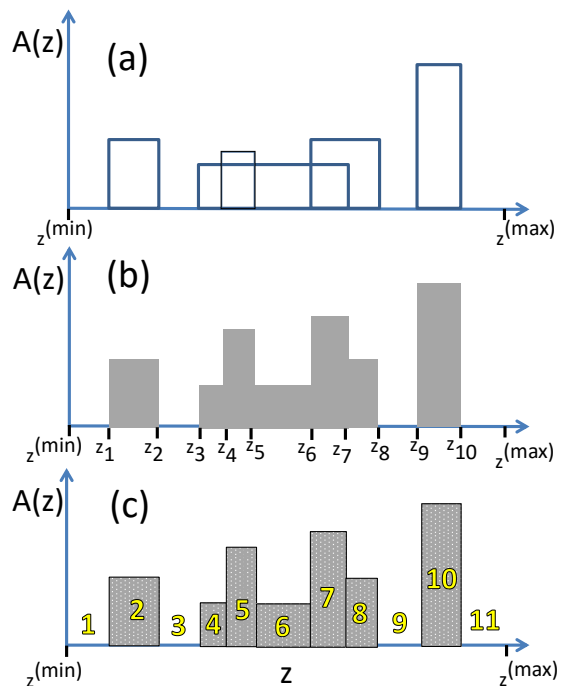


FIG. 2. (a) Spectral function parametrization by a set of rectangles. (b) Illustration of the treatment of intersections of rectangles. (c) Identical re-parametrization of the spectrum.

Updates proposing small modifications of the shape (“elementary” updates) have the disadvantage of long computation time for a basic solution. To speed up the

search, we supplement the standard protocol of Refs. 1 and 2 with consistent-constraints (CC) updates, which propose a radical shape modification based on minimization of the positive-definite quadratic form $\chi^2 + \sum_i o_i$ by matrix inversion as described in Ref. 3. Here o_i are various positive-definite quadratic forms, or “penalties,” that ensure that the matrix to be inverted is well-defined. This is achieved by penalizing the derivatives of $A(z)$ (computed on the grid based on the current configuration $\{\mathcal{C}\}$, see below) and enforcing $A(z) \geq 0$. The CC-update involves a number of iterations when penalties o_i are adjusted self-consistently in such a way that at the end of the update $0 < \sum_i o_i \ll \chi^2$. Explicit forms for $\{o_i\}$ and the adjustment protocols are described in detail in Ref. 3 (see also O_1 and O_4 forms in subsection IIB).

Even though the CC-updates do not compromise the goal of minimizing χ^2 , their efficiency is based on penalties that suppress saw-tooth fluctuations. To exclude possible bias originating from CC-updates on basic solutions we proceed as follows. The global update of the SOCC method consists of thousands of elementary updates L_{tot} that are divided into two groups: L_a stage-a updates and L_b stage-b updates, where $L_a + L_b = L_{\text{tot}}$ and $L_a < L_b$. Updates increasing χ^2 are temporarily considered “accepted” (and the resulting configuration recorded) with high probability during stage-a, but this probability is reduced during stage-b that favors updates decreasing χ^2 . The idea is to use L_a updates to escape from the local minimum of χ^2 in the multi-dimensional configuration space in a hope to find a better minimum afterwards. The global update is accepted only if a smaller value of χ^2 was recorded in the course of applying elementary updates, and the new configuration becomes the one with the smallest χ^2 . We apply CC-updates during stage-a of a global update when the increase of χ^2 is allowed, and proceed with a large number of elementary updates, which results in a configuration with fully developed saw-tooth instability.

We found that CC-updates have no effect on the self-averaging of the saw-tooth noise in the equal-weight superposition of basic solutions, improve typical χ^2 -values for basic solutions, and significantly decrease the computation time required for finding basic solutions.

To run the CC-update, one has to re-parameterize the configuration as a collection of nonoverlapping rectangles in order to be able to use their heights for estimates of the function derivatives. Panel (b) in Fig. 2 illustrates how overlaps of rectangles are understood in the SOCC method. This leads to an identical re-parametrization in terms of nonoverlapping rectangles $\{\tilde{P}_r\} = \{\tilde{h}_r, \tilde{w}_r, \tilde{c}_r\}$. The conversion is done as follows. First, the set of rectangle parameters $\{c_r - w_r/2\} \cup \{c_r + w_r/2\}$ is ordered to form a grid of new bin boundaries that also include the support limits $z^{(\min)}$ and $z^{(\max)}$. Second, bin centers and widths become centers and widths of the ordered set of

new rectangles, respectively:

$$\tilde{c}_{r+1} > \tilde{c}_r \quad \forall r, \quad (16)$$

$$\begin{aligned} \tilde{c}_1 - \tilde{w}_1/2 &= z^{(\min)}, \\ \tilde{c}_r - \tilde{w}_r/2 &= \tilde{c}_{r-1} + \tilde{w}_{r-1}/2 \quad \forall r, \\ \tilde{c}_{2R+1} + \tilde{w}_{2R+1}/2 &= z^{(\max)}. \end{aligned} \quad (17)$$

Figures 2(b) and 2(c) illustrate how the conversion from $\{P_t\}$ to $\{\tilde{P}_t\}$ amounts to an identical representation of the spectrum: R original rectangles introduce $2R$ boundaries on the $[z^{(\min)}, z^{(\max)}]$ interval and split it into $2R + 1$ rectangles obeying conditions (16)–(17). Note that some rectangles have zero height when submitted into the CC-update. The update modifies the values of all \tilde{h} -parameters and generates a new set $\{\tilde{h}'_r\}$. Since $\{\tilde{P}_r\}$ is a particular case of $\{P_r\}$, there is no need to perform any additional transformation to proceed with elementary updates.

B. Preparing the final solution

Because all basic solutions satisfy Eq. (1), one can immediately check that a linear combination of basic solutions, Eq. (9), always leads to a solution of Eq. (1) with the same accuracy cutoff χ_c as the basic solutions, provided that all c -coefficients are non-negative. Indeed, by linearity of the problem and the condition $\sum_{j=1}^J c_j = 1$,

$$\begin{aligned} G[n, A_{\text{fin}}] &= \sum_{j=1}^J c_j G[n, A_j], \\ g_n - G[n, A_{\text{fin}}] &= \sum_{j=1}^J c_j (g_n - G[n, A_j]). \end{aligned} \quad (18)$$

Substituting these expressions into the χ^2 form for the final solution and employing the Cauchy–Bunyakovsky–Schwarz inequality for $\chi_{jj'}$ we get

$$\chi^2 = \sum_{j,j'=1}^J c_j c_{j'} \chi_{jj'} \leq \bar{C}^2 \chi_c^2, \quad \text{with } \bar{C} = \sum_{j=1}^J |c_j|, \quad (19)$$

$$\chi_{jj'} = N^{-1} \sum_{n=1}^N \frac{(g_n - G[n, A_j])(g_n - G[n, A_{j'}])}{\delta_n^2}. \quad (20)$$

If some c -coefficients are negative, the accuracy of the final solution is guaranteed only if \bar{C} is not large. One may argue that the upper bound $\chi^2 \leq \bar{C}^2 \chi_c^2$ is substantially overestimating deviations, and the actual accuracy is better. Let $C_+ = (1 + \bar{C})/2$ and $C_- = (1 - \bar{C})/2$ be the sums over all positive and all negative coefficients, respectively. Then linear superpositions of basic solutions involving only positive and only negative coefficients and divided by C_+ and C_- (we denote them as A_+ and A_- , respectively), have their χ^2 measures smaller or equal to χ_c^2 , by Eq. (19). The final solution can be identically written as $A_{\text{fin}} = C_+ A_+ + C_- A_-$, and its χ^2 -measure is

nothing but the two state version of Eq. (19). Since the $G[n, A]$ values are derived from spectral density integrals they are smooth functions of n and random point-to-point sign fluctuations of $g_n - G[n, A]$ are arising predominantly from g_n . Thus, the expectation is that χ_{+-} is positive, in which case

$$\chi^2 \leq (C_+^2 + C_-^2)\chi_c^2 - 2C_+|C_-|\chi_{+-} \leq \frac{1 + \bar{C}^2}{2}\chi_c^2. \quad (21)$$

In practice, sign-positivity of the spectral density severely restricts the possibility of having large $|C_-|$ and \bar{C} in the final solution and $|C_-|$ tends to remain smaller than unity automatically. Finally, Eq. (19) is only an upper bound, and superpositions with \bar{C} as large as 2 may still have $\chi^2 < \chi_c^2$.

These considerations lead to an important possibility of modifying the shape of the final solution in order to satisfy additional criteria formulated outside of Eq. (1). The key observation, and crucial difference to other NAC methods, is that “conditional knowledge” protocols are invoked *after* all basic solutions are determined, meaning that they remain unbiased with respect to the input data.

As discussed in the Introduction, the most conservative philosophy regarding sharp spectral features, such as peaks and gaps, is to eliminate them if they are not warranted by the quality of the input data. (Our method does allow to answer the question whether a given sharp feature is compatible with the input data, see below.) To implement the idea, we formulate the problem of determining an appropriate set of $\{c_j\}$ coefficients as a linear self-consistent optimization problem closely following the consistent constraints method of Ref. 3. The objective function to be minimized consists of several terms, $O = \sum_{k=1}^5 O_k$, each being a quadratic positive-definite form of c_j . More terms can be added if necessary to control higher-order derivatives, enforce expected asymptotic behavior, etc.

- To suppress large derivatives we consider the following form

$$O_1 = \sum_{k=2}^K \{D_k^2[A'(z_k)]^2 + B_k^2[A''(z_k)]^2\}, \quad (22)$$

where $\{z_k\}$ is the grid of points used to define the first and second discrete derivatives of the function $A(z)$. The sets of coefficients D_k and B_k are adjusted under iterations self-consistently in such a way that contributions of all z_k -points to O_1 are similar.

- The unity-sum constraint on the sum of all coefficients in the superposition is expressed as

$$O_2 = \mathcal{U} \left(\sum_{j=1}^J c_j - 1 \right)^2, \quad (23)$$

with a large constant \mathcal{U} .

- Since $O_1 + O_2$ does not constrain the amplitudes and signs of all c_j the minimization cannot proceed by matrix inversion. To improve matrix properties we add a “soft” penalty for large deviations of c_j from the equal-weight superposition

$$O_3 = \sum_{j=1}^J (c_j - 1/J)^2. \quad (24)$$

- To ensure that the spectral function is non-negative (with high accuracy) we need z -dependent penalties (to be set self-consistently) that suppress the development of large negative fluctuations:

$$O_4 = \sum_{k=1}^K Q_k A(z_k)^2. \quad (25)$$

- Finally, we can introduce a penalty for the solution to deviate from some “target” function (or “default model”) $A_T(z_k)$:

$$O_5 = \sum_{k=1}^K T_k [A(z_k) - A_T(z_k)]^2. \quad (26)$$

The main purpose of O_5 is to address subtle multi-point correlations between allowed shapes: by forcing the solution to be close to a certain target function one can monitor how the solution starts developing additional saw-tooth-instability-related features or violates the unity-sum constraint. This penalty is zero when preparing A_{fin} in the absence of any target function.

The self-consistent optimization protocol is as follows. We start with $c_j = 1/J$ and compute $A(z_k)$. The initial sets of coefficients in O_1 are defined as $D_k = \mathcal{D}$, and $B_k = \mathcal{D}$, where \mathcal{D} is some small positive constant (its initial value has no effect on the final solution because penalties for derivatives will be increased exponentially under iterations). Since the positivity of $A(z)$ is guaranteed in the initial state, we set $Q_k = 0$. After the quadratic form for the objective function O is minimized, the new set of c -coefficients is used to define a new solution $A(z)$, penalties for derivatives are increased, $\mathcal{D} \rightarrow f\mathcal{D}$, $D_k \rightarrow fD_k$, $B_k \rightarrow fB_k$ by some factor $f > 1$, and then all penalties in O_1 and O_4 are adjusted self-consistently as follows:

- If $D_k|A'(z_k)| > \mathcal{D}$, we assign $D_k = \mathcal{D}/|A'(z_k)|$;
- If $B_k|A''(z_k)| > \mathcal{D}$, we assign $B_k = \mathcal{D}/|A''(z_k)|$;
- If $A(z_k) < 0$, we assign a large penalty suppressing the amplitude of the solution at this point, $Q_k = \mathcal{Q}$, where \mathcal{Q} is a large constant; otherwise the value of Q_k is increased by two orders of magnitude.

In this work we use $\mathcal{U} = 10^6$, $\mathcal{Q} = 10^6$, and $f = 2$. This sets the stage for the next iteration of the O -optimization protocol.

Since the accuracy expression, Eq. (18), relies on the substitution $g_n = \sum_{j=1}^J c_j g_n$, it is crucial that the unity-sum constraint is satisfied for all input data points,

$$\left| \sum_{j=1}^J c_j - 1 \right| < \epsilon, \quad \epsilon = \min\{|\delta_n/g_n|\}_n. \quad (27)$$

This provides the required criterion for terminating iterations. The final solution (9) is based on the last set of c -coefficients that satisfied the condition $\chi^2 < \chi_c^2$.

In the absence of the target objective O_5 , the procedure is guaranteed to produce a final solution $A_{\text{fin}}(z)$ with smooth behavior because our initial solution already satisfies all requirements. The derivative objective is forcing $A(z)$ to be as smooth as possible within the subspace of fluctuations that keep χ^2 small.

With the help of O_5 one can explore how the solution is modified if one forces it to go through some set of points.³ The simplest case would be to set $T_k = \mathcal{T}$ for some point z_o (where \mathcal{T} is a large number; in this work $\mathcal{T} = 10^6$) and zero otherwise, and shift $A_T(z_o)$ away from $A_{\text{fin}}(z_o)$. The solution going through the point $A_T(z_o)$ is no longer guaranteed to be smooth in the vicinity of z_o and for large deviations from the final solution will develop the saw-tooth instability at z_o .

The most interesting choices for z_o are the minima and maxima of the spectrum. Despite the fact that our protocol is to erase sharp features not warranted by the input data quality, we can still address questions such as “can this spectral peak (or gap) be made narrower/higher/lower and by how much, before the solution becomes unstable against developing secondary features?” This question cannot be fully answered at the level of the correlation matrix (8) because (i) spectral functions have subtle multi-point correlations, and (ii) the notion of a “typical” solution has no physical meaning in this context. The only way to answer this question is to have access to a large representative set of unbiased basic solutions.

The objective O_5 offers a generic way of exploring various possibilities for underlying features hidden behind the accuracy of input data. Clearly, there are other alternatives for addressing specific questions. For example, one can isolate a spectral peak to some interval and compute the dispersion d_j of each basic solution j over this interval. Next, the distribution function $W(d)$ over all basic solutions is composed and analyzed. If $W(d)$ has a narrow region of support around its average $\langle d \rangle$ value, then the peak width cannot significantly deviate from $\langle d \rangle$. If $W(d)$ is nonzero for $d \ll \langle d \rangle$ then one has to conclude that the actual peak might be much narrower (and, correspondingly, have a much higher amplitude) than what is predicted by the typical smooth solution A_{fin} .

III. MAXIMUM ENTROPY METHOD

Numerous NAC schemes are based on a totally different philosophy and impose additional restrictions/penalties on the allowed functional shapes of $A(z)$ in the process of solving Eq. (1). In other words, the search for solutions is biased with “conditional knowledge” from the very beginning. Historically, the Tikhonov-Phillips regularization method^{19–22} was the first to advocate this approach. Currently, the most popular scheme of this type is the maximum entropy method.^{4–9} Other schemes worth mentioning are singular value decomposition,²³ non-negative least-squares,²⁴ stochastic regularization,²⁵ and averaging Padé approximants.^{26,27} In the stochastic sampling method of Refs. 8, 28–30, the remaining bias is in the form of the predetermined grid of frequency points, and the final solution is an average over a certain “thermal” ensemble (see also Ref. 31 for a further refinement). Fast effective modification of stochastic optimization (FESOM)³² also uses the predetermined grid of frequency points.

We now briefly review the maximum entropy method,⁷ which can be seen as a special case of stochastic sampling methods.^{28,30} Instead of minimizing χ^2 one constructs a functional $Q = \frac{1}{2}\chi^2 - \alpha S[A]$, where $S[A]$ is the “entropy” term. The positive parameter α is a Lagrange multiplier that can also be thought of as a “temperature” by analogy to classical statistics (note that our definition of χ^2 differs by a factor of N from the standard MEM formulation; this is, however, only a matter of convention). The entropy term $S[A]$ takes the form $S[A] = -\int dz A(z) \ln[A(z)/M(z)]$ with $M(z)$ being the default model. For very large values of α , the default model term dominates in Q , reflecting our ignorance about the system. For very low values of α , the “energy” term χ^2 dominates, reflecting the quality of the input data. For intermediate values of α , one interpolates between these two limits and obtains a trade-off between accuracy and smooth behavior enforced by the default model. We are using Bryan’s method⁵ to implement the minimization procedure: the final answer is obtained by averaging over all values of α weighted with the respective *a posteriori* probability (we saw however little difference between Bryan’s method and the classical MEM in the examples below). In Bryan’s method, a singular value decomposition is also applied, which reflects the fact that the finite precision of storing floating point numbers in combination with the poor conditioning of the kernel puts severe limitations on the information that can possibly be retrieved. One can hence reduce the search space at no substantial loss; in practice, only 5 to 20 search directions survive this step. The remaining minimization is performed by the Levenberg-Marquadt algorithm. Bryan’s method is, after 25 years, still the *de facto* standard for inversion problems in condensed matter physics. One of its most attractive features is its speed: a few seconds on a laptop usually suffice to

get a reasonable answer provided good starting parameters (for the grid, default model, and the range of α) have been found. Nevertheless, the obtained answer (including the *a posteriori* probability distributions) should always be carefully checked.

A major issue is that the solution may strongly depend on the default model. (Note that the error bars which Ref. 7 calculates, are conditional on the default model and do hence not reflect variability with respect to different default models.) A practitioner usually wants to explore different (classes of) default models in order to get an idea of the robustness of the obtained answer, and sometimes to examine if lower values of χ^2 can be found for other solutions which are equally smooth. In this regard, all these solutions are reminiscent of basic solutions discussed above, but the probability density of solutions is different due to the difference in protocols: in the spirit of MEM one does not want default models that are too similar or default models that are too close to the obtained answer (an iteration where the new default model is the answer from a previous run, is considered a self-defeating strategy). This raises an important question of what strategy should be used to produce a representative set of basic solutions within MEM. One possibility is stochastic exploration of the configuration space of default models.

IV. PERFORMANCE TESTS

We perform blind tests of our method for two different kernels. The function $g(\tau_n)$ was prepared from equation (1) and uncorrelated Gaussian noise was afterwards added to $g(\tau_n)$.

A. Resolving the width of the high-energy peak

In this subsection, we assume that the spectral function $A(z)$ is identically equal to zero at $z < 0$, non-negative at $z > 0$, and the kernel is $K(\tau_n, z) = e^{-z\tau_n}$, see Eq. (2).

The spectral function for test 1 and test 2 (shown in Fig. 1) contains two peaks of finite width and has the following form (up to a normalization constant)

$$A(z) = \frac{c_1}{\sigma_1} \exp\left\{-\frac{(z-z_1)^2}{2\sigma_1^2}\right\} + \frac{c_2}{\sigma_2} \exp\left\{-\frac{(z-z_2)^2}{2\sigma_2^2}\right\}, \quad (28)$$

where $z_1 = 0.74$, $c_1 = 0.62$, $\sigma_1 = 0.12$, $z_2 = 2.93$, $c_2 = 0.41$, and $\sigma_2 = 0.064$. The spectrum is normalized to unity before adding uncorrelated Gaussian noise with relative standard deviation $\sigma = 10^{-3}$ for test 1 and $\sigma = 10^{-5}$ for test 2.

In the spectrum for test 3 the low-frequency peak is not a Gaussian but a δ -function with the same position

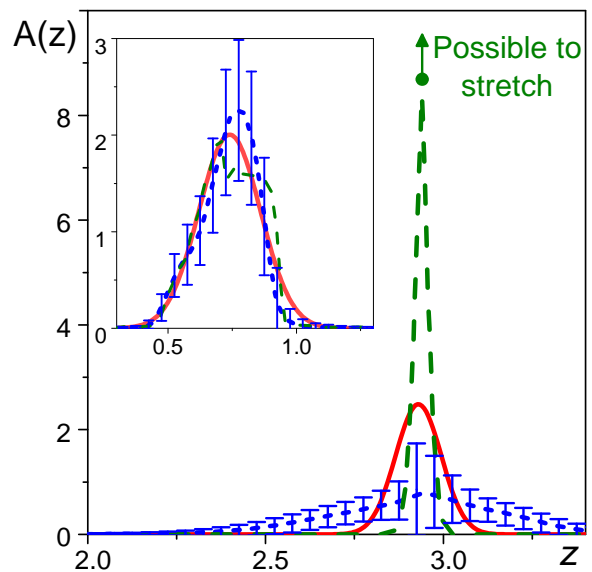


FIG. 3. (Color online.) Results for test 1, featuring two peaks of finite width with noise level 10^{-3} . Shown is the comparison between the actual spectrum (red solid line), the smooth SOCC spectrum (blue short-dashed line), and the pulled-up high-energy peak SOCC solution (green dashed line). The error bars for the smooth SOCC spectrum $\{\sigma_m\}$ are determined from Eq. (7).

and weight,

$$A(z) = \sqrt{2\pi} c_1 \delta(z-z_1) + \frac{c_2}{\sigma_2} \exp\left\{-\frac{(z-z_2)^2}{2\sigma_2^2}\right\}, \quad (29)$$

where $z_1 = 0.74$, $c_1 = 0.62$, $z_2 = 2.93$, $c_2 = 0.41$, and $\sigma_2 = 0.064$. The relative standard deviation of the uncorrelated Gaussian noise is $\sigma = 10^{-5}$.

The challenge for NAC is to judge whether one can resolve the width of the high-frequency peak. To this end we consider two possible setups for MEM and SOCC. In the standard setup we assume a flat default model for MEM and the SOCC procedure of generating smooth solutions as described in Sec. II B in the absence of the default model penalty O_5 . To study possible deformations of the second peak, we then introduce a narrow-peak default model in MEM and re-run the simulation, or, in the case SOCC, we insist that the final solution goes through a much higher point at the peak maximum. The width of the high-frequency peak is deemed impossible to resolve if one can reduce it by a factor of two, while the spectrum remains well-defined.

We note that better reproducibility of the low-frequency peak is a particular property of the kernel (2). For example, for the analytic continuation of the current-current correlation function to the optical conductivity, the main challenge is to resolve the spectral density at zero frequency.³³

Analysis of test 1 shows that the low-energy peak can be well resolved by both SOCC and MEM (see the insets

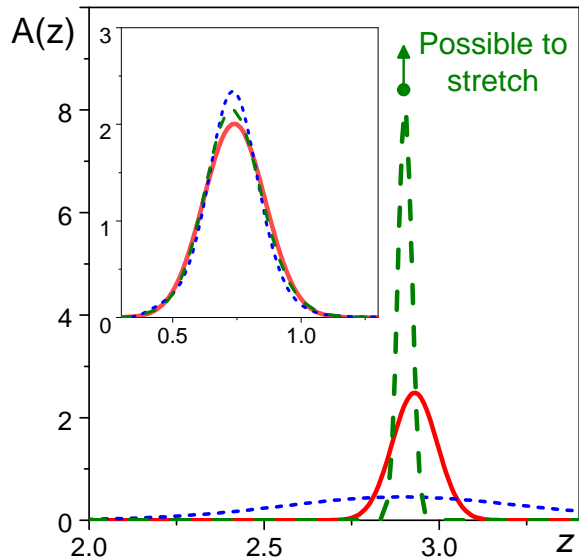


FIG. 4. (Color online.) Results for test 1, featuring two peaks of finite width with noise level 10^{-3} . Shown is the comparison between the actual spectrum (red solid line), the MEM spectrum with a flat default model (blue short dashed line), and the MEM spectrum with a pulled-up high-energy peak in the default model (green dashed line).

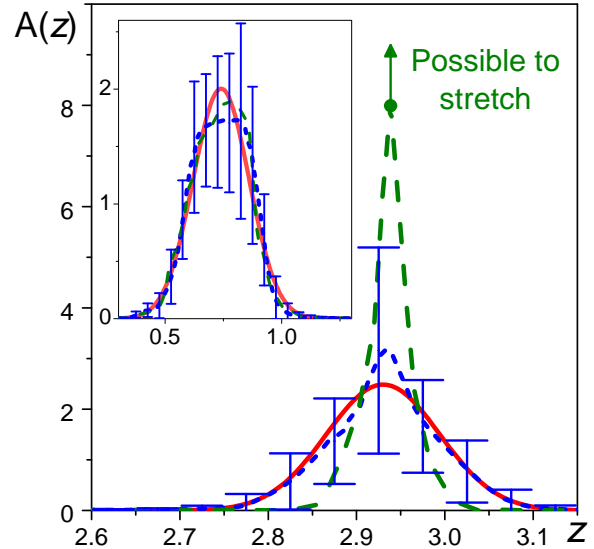


FIG. 6. (Color online.) Results for test 2, featuring two peaks of finite width with noise level 10^{-5} . Shown is the comparison between the actual spectrum (red solid line) and the smooth SOCC spectrum (blue short-dashed line), the pulled-up high-energy peak SOCC solution (green dashed line). The error bars for smooth SOCC spectrum $\{\sigma_m\}$ determined from Eq. (7).

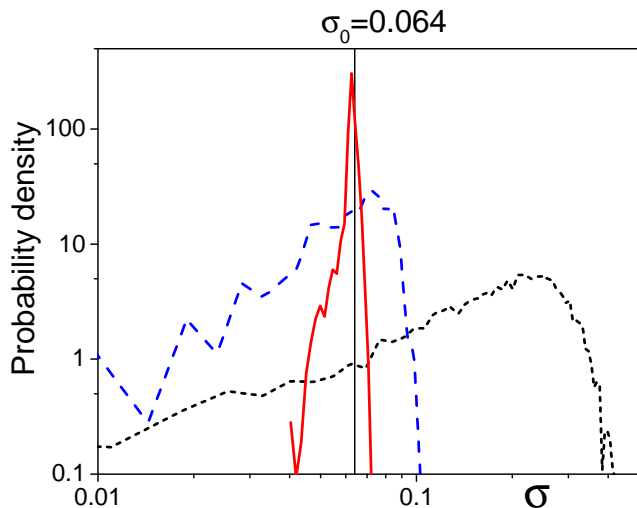


FIG. 5. (Color online.) Distribution of the second moment for the high frequency peak in test 1 (short-dashed black line), test 2 (dashed blue line), and test 3 (red solid line), among all basic solutions. The vertical line shows the second moment $\sigma_0 = 0.064$ of the original spectrum.

in Figs. 3 and 4, respectively). On the other hand, the high-energy peak width is severely overestimated by both methods in the standard setup (Figs. 3 and 4). However, both methods allow one to pull the high-frequency peak up at least by a factor of four above the actual spectrum. Specifically, if the second peak in the MEM default model is set to be much narrower than the actual

one, then MEM produces an answer of the same width as this default model. Similarly, the superposition of basic SOCC solutions can be forced to have a much higher amplitude at the second peak maximum by employing an appropriate target function. In SOCC, one may also see direct evidence that the second peak width is questionable by considering statistics of the second moments σ for the high-frequency peak among all basic solutions. The corresponding distribution is presented in Fig. 5. The probability to find a solution with a vanishing width ($\sigma \rightarrow 0$) for the high-frequency peak does not go to zero for test 1 and, hence, the imaginary-time data for $g(\tau_n)$ (within their accuracy) do not rule out a δ -function for the high-frequency peak.

Further insight is provided by test 2, which differs from test 1 only in the noise level, which is reduced by two orders of magnitude. One readily observes that, in contrast to test 1, the standard setups of SOCC and MEM give a very good description of the high-frequency peak (Figs. 6 and 7). Does this mean that one can be absolutely sure that the width of the peak is finite? The answer is no, because one can still easily pull the peak up by a factor of four. Moreover, SOCC analysis of second moments (see Fig. 5) demonstrates that a δ -functional shaped second peak is still a possibility, despite improved error bars. In these examples, tighter error bars allow only to reduce the upper bound on the width of the second peak. Much smaller error bars, which are unrealistic for Monte Carlo simulations of $g(\tau_n)$, would be required to controllably

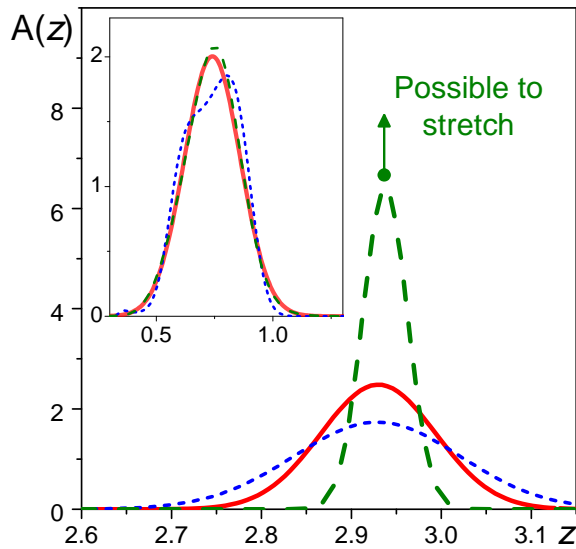


FIG. 7. (Color online.) Results for test 2, featuring two peaks of finite width with noise level 10^{-5} . Shown is the comparison between the actual spectrum (red solid line), MEM with a flat default model (blue short-dashed line), and MEM with a pulled-up high-energy peak in the default model (green dashed line).

resolve the actual width of the second peak.

Test 3 has the same Gaussian noise as test 2 but the low-frequency peak is now replaced by a δ -function, see Eq. (29). This crucially changes the results. Now the high-frequency peak is well reproduced not only in the standard setup of SOCC and MEM but also in attempts to pull the solution up, see Figs. 8 and 9, respectively. Stability of results for the second peak width is also evident in the probability distribution for the second moment shown in Fig. 5. The distribution is peaked at the correct value $\sigma_2 = 0.064$ and is rather narrow, indicating that a narrower peak would compromise the error bars.

We emphasize that the success of resolving the width of the second peak in test 3 is due to a combination of two circumstances: the small width of the first peak and the high accuracy of the input data. To see this, it is instructive to consider the physical example of the Fermi polaron (see Sec. V), where the width of the first peak is very small, but the accuracy of the input data is significantly lower than in test 3.

B. Fermi distribution kernel

Test 4 analyzes the possibility of resolving spectral densities at the Fermi level from the analytic continuation of $g(\tau)$. Here, the spectrum $A(z)$ is defined in the range $-\infty < z < \infty$ and the kernel is $K(\tau_n, z) = \exp\{-z\tau_n\}/(1 + \exp\{-z\beta\})$ with $\beta = 6$. The uncorrelated Gaussian noise is added at the 10^{-5} level. One

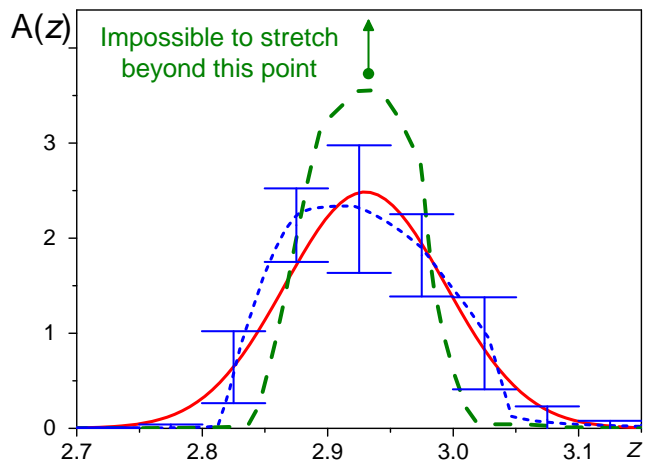


FIG. 8. (Color online.) Results for test 3, characterized by a δ -function at low frequency and a peak of finite width at high frequency with noise level 10^{-5} . Shown is the comparison between the actual spectrum (red solid line), the smooth SOCC spectrum (blue short-dashed line), and the maximally pulled-up high-energy peak SOCC solution (green dashed line). The error bars for smooth SOCC spectrum $\{\sigma_m\}$ determined from Eq. (7).

can see in Figs. 10 and 11 that both SOCC and MEM give a good description of the spectral function in the vicinity of the chemical potential (at $z = 0$). Also, the height of the middle peak at near zero frequency cannot be significantly pulled up without distorting the rest of spectrum. Specifically for MEM, trying different default models with one, two, or three Gaussian peaks did not improve the answer; in all cases trying to find narrower peaks resulted in secondary oscillations reminiscent of numerical instabilities. We conclude that the fermionic spectrum can be restored for the given parameters with high quality.

V. APPLICATION OF SOCC TO THE FERMI POLARON PROBLEM

We now test the SOCC method on a physical system—the resonant Fermi polaron (a spin-down fermion in a sea of noninteracting spin-up fermions)^{34,35}; here in three dimensions and for equal mass of spin-up and spin-down particles. The coupling between the polaron and its environment is characterized by a single dimensionless parameter $k_F a$, where k_F is the Fermi wave vector and a the s-wave scattering length. Here we examine a typical situation at $k_F a = 0.8$ when the polaron state at zero momentum is metastable but has a very long relaxation time, implying that the lowest peak in the polaron spectral function is a sharp resonance nearly indistinguishable from a δ -function.

The imaginary-time polaron Green's function at zero

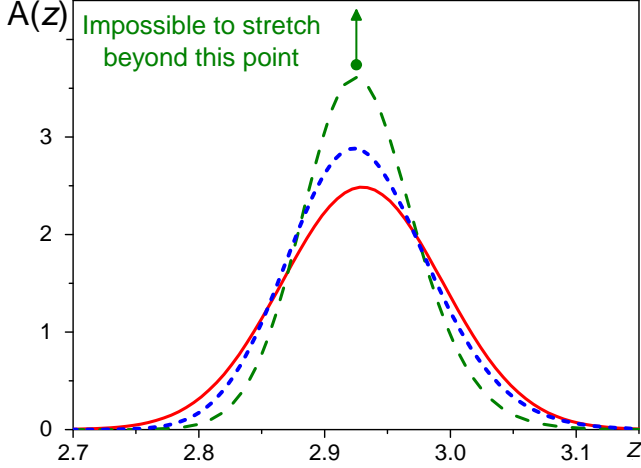


FIG. 9. (Color online.) Results for test 3, characterized by a δ -function at low frequency and a peak of finite width at high frequency with noise level 10^{-5} . Shown is the comparison between the actual spectrum (red solid line), the MEM spectrum with a flat default model (blue short-dashed line), and the MEM spectrum with a double Gaussian default model where the second peak is maximally pulled up (green dashed line).

temperature and zero momentum, $g_n = g(\tau_n)$, was obtained with diagrammatic Monte Carlo, see Refs. 1, 13, and 36. We are able to achieve very high precision in our results for $g(\tau)$ with a relative error as low as $\mathcal{O}(10^{-7} - 10^{-9})$ at τ close to zero, $\mathcal{O}(10^{-4} - 10^{-3})$ around $\tau = 1/\varepsilon_F$ (where ε_F is the Fermi energy of spin-up fermions) and a few percent at the largest τ considered for the analytic continuation. The kernel at zero temperature is $K(\tau_n, z) = e^{-z\tau_n}$.

The polaron spectral function features two peaks. The position and weight of the first polaron peak are fixed with high accuracy by the asymptotic decay of the Green's function, $-g(\tau \rightarrow \infty) \rightarrow Z_1 e^{-E_1 \tau}$. Our data at large $\varepsilon_F \tau_n$ can be fitted to a single exponential (within error bars) indicating that the polaron remains a well-defined quasi-particle in this parameter range. The particle-hole continuum emerges at higher frequencies as a second broad peak. A key question we want to address here is its spectral width. This has been discussed in the context of the repulsive polaron state.^{11,14-17} In order for it to qualify to be a well-defined quasiparticle, the peak width needs to be sufficiently narrow (much smaller than the Fermi energy, corresponding to a sufficiently long life time). Thus resolving the width accurately is very important to correctly interpret this spectrum. Note that this spectrum has the same general features as the spectrum for test 1 in the previous section.

When SOCC is used to produce a smooth solution the second peak emerges as a broad spectral feature. If this was indeed the case, the metastable repulsive polaron picture would be inapplicable for $k_F a = 0.8$. However,

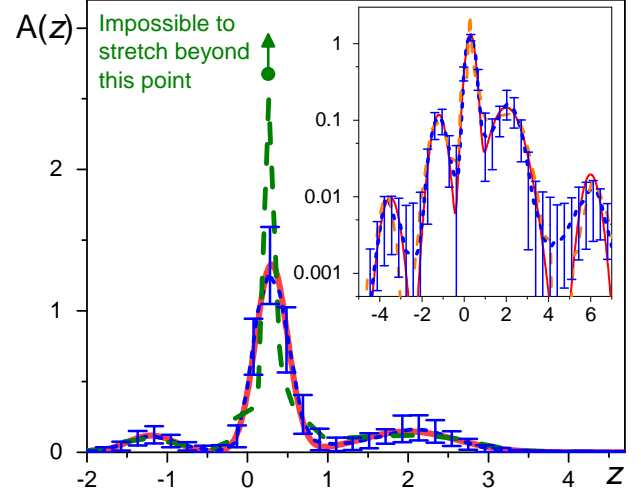


FIG. 10. (Color online.) Results for test 4 with a Fermi distribution kernel and noise level 10^{-5} . Shown is the comparison between the actual spectrum (red solid line), the smooth SOCC spectrum (blue short-dashed line), and the maximally pulled up central peak SOCC solution (dashed green line). The logarithmic plot in the inset highlights the comparison of low-intensity features. The error bars for the smooth SOCC spectrum $\{\sigma_m\}$ are determined from Eq. (7).

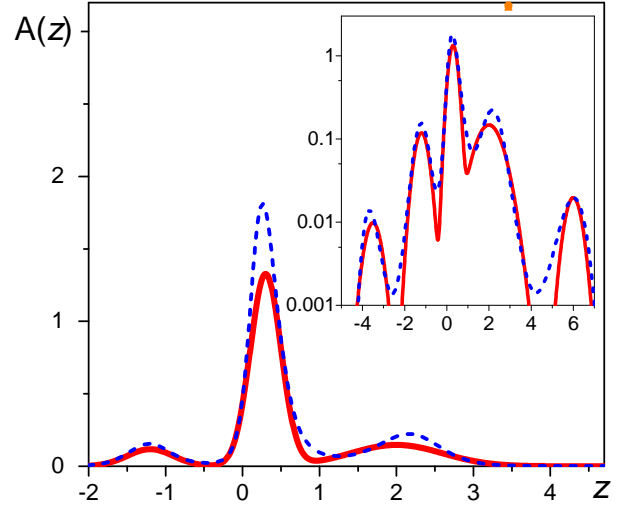


FIG. 11. (Color online.) Results for test 4 with a Fermi distribution kernel and noise level 10^{-5} . Shown is the comparison between the actual spectrum (red solid line) and the MEM spectrum in the default setup (blue dashed line).

the same set of basic solutions can be optimized to have a much narrower peak, see Fig. 12, implying that a well-defined repulsive polaron quasi-particle cannot be ruled out. Given that the second peak dispersion can be reduced by a factor of four without compromising the accuracy of the final solution, we have to conclude that the quality of the input data is insufficient to determine the

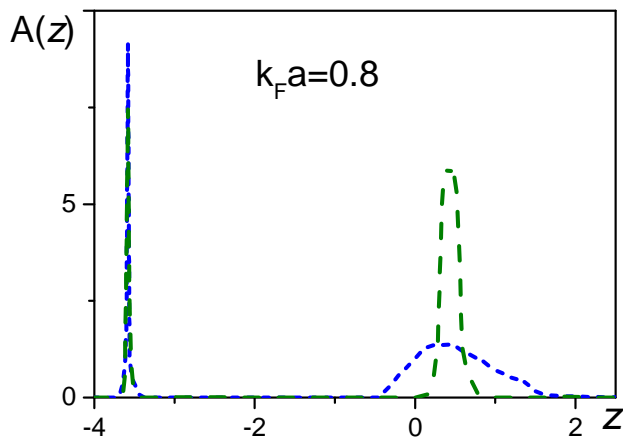


FIG. 12. (Color online.) Spectral density of the resonant Fermi polaron for $k_F a = 0.8$ at zero momentum and zero temperature. The smooth SOCC spectrum with the second peak dispersion $\sigma_2 = 0.48$ is shown by the blue short dashed line. However, a much narrower solution for the second peak with $\sigma_2 = 0.12$ (green dashed line) can also be obtained from the same set of basic solutions.

actual width.

VI. CONCLUSIONS

The most challenging aspect of numerical analytic continuation is not the algorithm of finding a stable (smooth) solution consistent with the input data, but the protocol of assessing its accuracy and unambiguity. We have implemented such a protocol based on the method of stochastic optimization with consistent constraints and demonstrated how a similar strategy can be followed with the maximum entropy method by exploring the space of default models. Irrespective of the method, the procedure has to deal with either integrals of the spectral function (rather than the function itself) and/or certain *a priori* and *a posteriori* constraints consistent with the error bars on the input data.

It is important to distinguish between two cases. The

first (simplest) case is when all physically meaningful solutions do not differ substantially, upon possible smearing of unimportant (below the resolution) fine details of the otherwise smooth spectral function. The second case, exemplified by the spectral function in Fig. 1, is when a piece of important physical information is inevitably lost. In the first case, a reasonable characterization of uncertainties can be achieved by coarse-graining, like, e.g., Eq. (3). In the second case, one has to employ a more elaborate approach to reveal the different possible physical solutions that do not compromise the error bars of the input data.

Much of our attention has been paid to the protocol of treating the second case. We have shown how it can be handled with SOCC and modified MEM. With MEM one has to explore various default models and resulting solutions that remain consistent with input error bars. A useful feature of the SOCC approach is that such an analysis—and, more generally, the application of all possible consistent constraints—can be implemented at the post-processing stage using a representative set of “basic” solutions generated by the stochastic-optimization protocol. The linearity of the problem (1) is crucial here, as it guarantees that any superposition of basic solutions with non-negative weights is also a solution to Eq. (1) within the same or better level of accuracy. Even if the superposition coefficients are allowed to be negative, the procedure typically keeps the accuracy of the final solution at the level of basic solutions. This allows one to implement consistent constraints by choosing the superposition coefficients to minimize the corresponding objective function.

Acknowledgements. This work was supported by the Simons Collaboration on the Many Electron Problem, the National Science Foundation under the grant PHY-1314735, the MURI Program “New Quantum Phases of Matter” from AFOSR, and FP7/ERC starting grant No. 306897. A.S.M. is supported by the ImPACT Program of the Council for Science, Technology and Innovation (Cabinet Office, Government of Japan). Our maximum entropy implementation builds on the ALPS implementation.³⁷

¹ A. S. Mishchenko, N. V. Prokof'ev, A. Sakamoto, and B. V. Svistunov, *Phys. Rev. B* **62**, 6317 (2000).
² A. S. Mishchenko, in *Verlag des Forschungszentrum Jülich*, 2012. - 978-3-89336-796-2, edited by E. Pavarini, E. Koch, F. Anders, and M. Jarrell (2012).
³ N. Prokof'ev and B. Svistunov, *JETP Lett.* **97**, 747 (2013).
⁴ R. N. Silver, D. S. Sivia, and J. E. Gubernatis, *Phys. Rev. B* **41**, 2380 (1990).
⁵ R. Bryan, *Eur. Biophys. J.* **18**, 165 (1990).
⁶ J. E. Gubernatis, M. Jarrell, R. N. Silver, and D. S. Sivia, *Phys. Rev. B* **44**, 6011 (1991).
⁷ M. Jarrell and J. E. Gubernatis, *Phys. Rep.* **269**, 133

(1996).
⁸ S. Fuchs, T. Pruschke, and M. Jarrell, *Phys. Rev. E* **81**, 056701 (2010); A. Dirks, P. Werner, M. Jarrell, and T. Pruschke, *Phys. Rev. E* **82**, 026701 (2010).
⁹ O. Gunnarsson, M. W. Haverkort, and G. Sangiovanni, *Phys. Rev. B* **81**, 155107 (2010); *ibid* *Phys. Rev. B* **82**, 165125 (2010).
¹⁰ A. Schirotzek, C.-H. Wu, A. Sommer, and M. W. Zwierlein, *Phys. Rev. Lett.* **102**, 230402 (2009).
¹¹ C. Kohstall, M. Zaccanti, M. Jag, A. Trenkwalder, P. Massignan, G. M. Bruun, F. Schreck, and R. Grimm, *Nature* **485**, 615618 (2012).

- ¹² M. Koschorreck, D. Pertot, E. Vogt, B. Fröhlich, M. Feld, and M. Köhl, *Nature* **485**, 619622 (2012).
- ¹³ O. Goulko, A. S. Mishchenko, N. Prokof'ev, and B. Svistunov, arXiv:1603.06963.
- ¹⁴ M. Parish, and J. Levinsen, arXiv:1608.00864.
- ¹⁵ K. Kamikado, T. Kanazawa, and S. Uchino, arXiv:1606.03721.
- ¹⁶ R. Schmidt and T. Enss, *Phys. Rev. A* **83**, 063620 (2011).
- ¹⁷ P. Massignan, and G. M. Bruun, *Eur. Phys. J. D* **65**, 83 (2011).
- ¹⁸ Such a statistical treatment of multiple independent solutions was first suggested in the fast modification of SOM method, see Ref. 32
- ¹⁹ A. N. Tikhonoff, *Doklady Akademii Nauk SSSR*, **39**, 195 (1943); *ibid* **151**, 501 (1963) [*Soviet Mathematics* **4**, 1035 (1963)].
- ²⁰ D. L. Phillips, *J. ACM* **9**, 84 (1962).
- ²¹ A. N. Tikhonoff and V.Y. Arsenin, *Solutions of Ill-posed Problems* (Winston & Sons, Washington, 1977).
- ²² A. N. Tikhonov, A. Goncharky, V. V. Stepanov, and A. Yagola, *Numerical Methods for the Solution of Ill-posed Problems* (Springer-Science+Business Media, B.V., Moscow, 1995).
- ²³ C. E. Creffield, E. G. Klepfish, E. R. Pike, and S. Sarkar, *Phys. Rev. Lett.* **75**, 517 (1995).
- ²⁴ C. L. Lawson and R. J. Hanson, *Solving Least Squares Problems*, Society for Industrial and Applied Mathematics, Philadelphia, 1995.
- ²⁵ I. S. Krivenko and A. N. Rubtsov, *JETP Lett.* **94**, 768 (2012).
- ²⁶ J. Schött, I. L. M. Locht, E. Lundin, O. Grånäs, O. Eriksson, and I. Di Marco, *Phys. Rev. B* **93**, 075104 (2016).
- ²⁷ J. Schött, E. G. C. P. van Loon, I. L. M. Locht, M. Katsnelson, and I. Di Marco, arXiv:cond-mat/1607.04212.
- ²⁸ A. W. Sandvik, *Phys. Rev. B* **57**, 10287 (1998).
- ²⁹ K. Vafayi and O. Gunnarsson, *Phys. Rev. B* **76**, 035115 (2007).
- ³⁰ K. S. D. Beach, arXiv:cond-mat/0403055.
- ³¹ A. W. Sandvik, arXiv:1502.06066.
- ³² T. A. Maier, private communication.
- ³³ A. S. Mishchenko, N. Nagaosa, G. De Filippis, A. de Candia, and V. Cataudella, *Phys. Rev. Lett.* **114**, 146401 (2015).
- ³⁴ P. Massignan, M. Zaccanti, and G. M. Bruun, *Rep. Prog. Phys.* **77**, 034401 (2014).
- ³⁵ Z. Lan and C. Lobo, *J. Indian I. Sci.* **94**, 179 (2014).
- ³⁶ N. Prokof'ev and B. Svistunov, *Phys. Rev. B* **77**, 020408 (2008); *ibid* *Phys. Rev. B* **77**, 125101 (2008).
- ³⁷ B. Bauer *et al.*, *Journal of Statistical Mechanics: Theory and Experiment*, P05001 (2011).